

THE IDENTIFICATION OF INFRARED SYNCHROTRON RADIATION FROM CASSIOPEIA A

T. J. JONES¹, L. RUDNICK, T. DELANEY & J. BOWDEN
 Astronomy Department, University of Minnesota, Minneapolis, MN 55455

Draft version December 20, 2018

ABSTRACT

We report the discovery of polarized flux at 2.2 μ m from the bright shell of the \approx 320 year old supernova remnant Cas A. The fractional polarizations are comparable at 6 cm and 2.2 μ m, and the polarization angles are similar, demonstrating that synchrotron radiation from the same relativistic plasma is being observed at these widely separated wavebands. The relativistic electrons radiating at 2.2 μ m have an energy of \approx 150 GeV, ($\gamma \approx 3 \times 10^5$), assuming an \approx 500 μ G magnetic field. The total intensity at 2.2 μ m lies close to the power law extrapolation from radio frequencies, showing that relativistic particle acceleration is likely an ongoing process; the infrared emitting electrons were accelerated no longer than \approx 80 years ago. There is a small but significant concave curvature to the spectrum, as expected if the accelerating shocks have been modified by the back pressure of the cosmic rays; given calibration uncertainties, this conclusion must be considered tentative at present. The 2.2 μ m polarization angles and the emission-line filaments observed by HST are both offset from the local radial direction by 10 – 20 degrees, providing evidence that the magnetic fields in Cas A are generated by Rayleigh-Taylor instabilities in the decelerating ejecta.

Subject headings: acceleration of particles — magnetic fields — polarization — radiation mechanisms: nonthermal — supernova remnants

1. INTRODUCTION

The energy distribution of \approx 0.1 – 10 GeV electrons in supernova remnants has been studied for decades through their radio synchrotron radiation. The distributions are typically power laws, with low energy spectral flattenings often seen due to absorption in the interstellar medium (Kassim 1989), or perhaps even due to internal ionized gas in the case of Cas A (Kassim et al. 1995). The power law slopes (spectral indices) vary significantly from remnant to remnant (Green 2001). Although it has long been accepted that diffusive shock acceleration is responsible for the GeV electrons (Bell 1978), there are still no clear observational signatures for how this is regulated in different remnants. Spectral index variations within an individual remnant are often very small; this presents a dilemma because the asymmetries in remnant structures and dynamics should lead to large variations in spectral index if particle acceleration is due to first-order Fermi acceleration at shocks. In older remnants, such as the Cygnus Loop, spectral variations probably reflect local differences in absorption and confusion along the line of sight (Leahy & Roger 1998). But in Cas A, the spectral variations across the remnant (Anderson & Rudnick 1996) are most consistent with different power laws, indicating local variations in relativistic particle acceleration (Wright et al. 1999). Information about deviations from the power law shape could provide important information about the acceleration mechanisms and the possible modifications of the shocks by cosmic-ray backpressures (Berezhko & Ellison 1999); only weak evidence for such deviations exists to

date (Reynolds & Ellison 1992).

The maximum energy to which cosmic rays can be accelerated in supernova remnants is another issue of current importance. Non-thermal X-ray synchrotron radiation from the supernova remnants SN1006 (Koyama et al. 1995; Reynolds 1996), RX J1713.7-3946 (Koyama et al. 1997; Slane et al. 1999), Cas A (Allen et al. 1997), and RCW86 (Borkowski et al. 2001) suggest that relativistic electrons have energies up to 100 TeV. Gamma-ray detections of SN1006 (Tanimori et al. 1998) and RX J1713.7-3946 (Muraishi et al. 2000) have been interpreted as the Inverse Compton emission from these high energy electrons against the cosmic microwave background.

Although the energies of electrons that would produce synchrotron radiation in the infrared are considerably lower than those emitting X-rays and γ -rays, they offer the possibility of a model-independent probe of electrons at much higher energies than seen in the radio. The possibility of near or mid-IR synchrotron emission was first suggested to us by R. Tuffs (private communication and Tuffs et al. (1997)), based on their impressions of the ISOCAM images (Lagage et al. 1996). The possibility was again raised by Gerardy & Fesen (2001), who noted the close similarity between their 2.2 μ m (but not 1.2 μ m) image and the radio images. This led us to seek verification of the infrared synchrotron origin through polarization measurements.

2. OBSERVATIONS

2.1. *Choice of Field*

¹ Visiting Astronomer at the Infrared Telescope Facility, which is operated by the University of Hawaii under contract from the National Aeronautics and Space Administration.

The observations were made using NSFCAM on the IRTF in polarimetry mode on 1 August, 2001. Since NSFCAM has a field of view of about 75" (0.3" per pixel) and we would have time to observe only one field, we had to make a careful choice of location within the Cas A remnant. The 2.2 μm band image kindly provided by C. Gerardy and R. Fesen (Gerardy & Fesen 2001) gave us information on the flux from Cas A at 2.2 μm . Our own radio images of Cas A (Anderson & Rudnick 1996; Anderson, Keohane & Rudnick 1995; Gotthelf et al. 2001) provided us with total intensity and polarized intensity maps that could be compared to the 2.2 μm band image.

Our choice of which region in Cas A to observe was influenced by a number of factors. First, there had to be a good correspondence between the radio synchrotron emission and the 2.2 μm emission. This was done to avoid small bright regions of emission at 2.2 μm that might be contaminated by emission lines unrelated to the radio synchrotron emission. Second, there had to be significant polarized intensity in the radio, which we hypothesized would correspond to similar polarization in the near infrared. Third, there had to be sufficient flux at 2.2 μm to make fractional polarization measurements of a few percent, a level similar to the observed radio polarization. Using these criteria, we chose a segment of Cas A's bright ring in the northwest (azimuths of ≈ 0 to -40 degrees) centered at RA 23h 23m 26s, Dec 58°, 48' 58.4", (J2000), as shown in Figure 1.

2.2. Polarization Observations

The techniques for using NSFCAM as an imaging polarimeter are described in Jones (1997, 2000). Images are taken of the source and an off-source sky location at four positions of a half waveplate that can be rotated in the beam. This allows us to form sky subtracted intensity images at polarization position angles of 0, 45, 90 and 135° (waveplate angles of 0, 22.5, 45 and 67.5°). We formed two independent estimates of the total intensity ($I_0 + I_{90}$) and ($I_{45} + I_{135}$), and found that these were consistent with each other within the off-source noise errors. Photometric calibration was done using observations of HD 225023 from the Elias standards list (Elias et al. 1982). The 2.2 μm (K) intensity scale was set using the conversion $0.0 m_K = 635$ Jy. The final accuracy of our spectral indices is limited by the 2.2 μm extinction corrections, as discussed below.

From the images at four angles, we then computed Stokes images Q ($I_0 - I_{90}$) and U ($I_{45} - I_{135}$) and the total intensity image $\frac{1}{2}(I_0 + I_{45} + I_{90} + I_{135})$. Note that these Stokes parameter definitions differ by a factor of two from those commonly used in the radio. The details of our sequencing of source, sky and waveplate position differed somewhat from Jones (1997). For Cas A we rotated back and forth between two waveplate positions (either for Q or U) for several minutes, then repeated the same procedure on the sky position. Integrations at a single waveplate position were 10 seconds. It took about 2 seconds for the waveplate to move to a new position.

NSFCAM is not a true imaging polarimeter, but rather a camera retrofitted with some polarization optics, so we were limited by systematics in the precision of our polarimetry to about $\pm 0.3\%$. This limit is due primarily to fluctuations in atmospheric transmission between the time it takes to integrate at different positions of the waveplate.

Since we are interested in polarizations of a few percent or more in Cas A, this instrumental limitation did not hinder our observations. In fact, the nebulosity in Cas A at 2.2 μm is sufficiently faint that our measurements are effectively photon noise limited by the background.

Calibration of the position angle was done using observations of AFGL 490 two nights earlier with the same observing procedure as for Cas A. AFGL 490 was assumed to have a polarization angle of $\theta = 115^\circ$ at 2.2 μm (Kobayashi et al. 1978). The Q' and U' values quoted in Table 1 are given as observed; the PA contains a -33 degree correction to place it in the proper sky frame. An extra check on the position angle calibration was done using observations on 1 August of the reflection nebulosity surrounding the young star RNO1 (Weintraub & Kastner 1993). The centrosymmetric scattering pattern around this star produces all possible position angles and provides a very sensitive calibration. Calibration of the efficiency (which exceeds 98% at 2.2 μm) was performed in previous observing runs using S1 in ρ Oph which has a polarization of 1.9% at 2.2 μm . Instrumental polarization was checked during the night by observing an unpolarized standard star from the UKIRT faint standards list (FS 149) and was found to be too small to be measured.

The telescope was offset 100" to the North for the sky frames. This was intended to move the telescope well off Cas A, but not so far that telescope movement and settling time seriously reduced our observing efficiency. In an effort to increase our time on Cas A itself, we reduced the number of background frames to about half the number of frames taken on the source. The total on source integration time was ≈ 1 hr. Serious telescope drift during the long integrations on Cas A resulted in the movement of stars in the background frames relative to the source frame. This produced elongated stars in the background subtracted images (see Figure 1, 2.2 μm intensity). No correction has been made for these problems, and the effect on our spectral measurements is described below. Our polarization measurements are less affected by the star trails than the total intensity because the star polarizations are expected to be $\approx 1\%$ as discussed below, while Cas A's polarization is $\approx 5 - 10\%$.

Since the time between source and background frames ranged over several minutes, fluctuations in sky background could cause a residual DC level to be present in the sky subtracted images. Although small compared to the net intensity of the brighter nebulosity in Cas A, this DC offset could be comparable to the polarized intensity, and produce a spurious net intensity in the Q and U images. These offsets were removed by first identifying several small regions of the sky-subtracted total intensity image with values fluctuating near zero for the intensity. We simply assume the true intensity is zero when averaged over these locations and subtract the respective means from the I, Q and U images to force them to be zero there. This procedure will remove the DC offset produced by sky background fluctuations in the Q and U images, but also would remove any real, but faint emission. Sensitive observations in the radio do show faint total intensity and polarized emission from these regions, at intensities of approximately 15% that of the bright ring; no correction has been made for this small bias.

2.3. Radio and Optical Images

The radio images were produced from observations at the Very Large Array² using all four configurations over the time period from May, 1997 through March, 1998. Maps were made by using the data from 1.285 GHz for the 20 cm band, and from 4.64 GHz for the 6 cm band. The flux calibration scale was set using standard VLA procedures (VLA Calibration Manual 2002) and the source 3C48. The polarization calibration also used standard VLA procedures with the angle fixed by assuming a position angle of -10° for 3C138. Other details of analysis and image creation are similar to those described by Anderson, Keohane & Rudnick (1995). The full resolution of these images was $\approx 1.5''$.

The optical emission in Cas A's bright ring is dominated by clumpy emission lines on a wide range of scales, most recently studied in great detail by Fesen et al. (2001). The emission line material represents a distinct temperature component, separate from the synchrotron plasma, but which may dominate the dynamics driving the relativistic particles and magnetic fields. In particular, Fesen et al. (2001) noted from their high resolution WFPC2 observations, a very large number of filamentary structures that they suggested were Rayleigh-Taylor instabilities. Although there is significant small-scale scatter, we measured the approximate position angle of the filaments at the azimuths of the boxes used for the synchrotron measurements and list these in Table 1.

3. DATA ANALYSIS & RESULTS

3.1. Image Registration

The registration of the $2.2\ \mu\text{m}$ and radio images was done in two steps. The radio coordinates from the VLA are already in the FK4 reference frame to an accuracy of $\approx 0.1''$. To put the $2.2\ \mu\text{m}$ image in the same frame, we first used the Sloan Digital Sky Survey to register the image of the entire Cas A field kindly provided by C. Gerardy & R. Fesen (Gerardy & Fesen 2001). We then minimized the rms differences between our new small polarimetry field and the Gerardy/Fesen image, allowing for shifts in position, rotation, and scale. The final accuracy of this registration is $< 0.1''$, and the uncertainties have no effect on the results discussed here.

3.2. Spatial averaging

The signal:noise on the $0.3''$ pixel level was not sufficient either for accurate spectral measurements or determination of the polarization. We therefore found the average brightness for I, Q, and U in each waveband in six boxes as shown in Figure 1, and listed in Table 1. These boxes were chosen to have sufficiently high polarized flux at 6 cm, to avoid regions with bright stars in the sky ("off") frame, and to avoid the edges of the frame where the flat fielding is less accurate.

For display purposes, we also convolved the polarizations (Q and U) to a resolution of $10''$. The resulting low resolution polarized intensities are shown on the right side of Figure 1. The middle image of the right side represents a prediction of the $2.2\ \mu\text{m}$ polarizations using the radio

data and $2.2\ \mu\text{m}$ total intensities. It was constructed by taking the fractional polarization image at 6 cm and multiplying it by the total intensity image at $2.2\ \mu\text{m}$. The overall correspondence is good, but not perfect. The $2.2\ \mu\text{m}$ polarized intensity map contains, e.g., a bright spot due to residuals from the bright star immediately to the SE of box 6. In addition, it has not been corrected for the noise bias, which is responsible for some of the structure in the image. The 6 cm polarization angles were used, after correction for Faraday rotation as described below, as a prediction for the $2.2\ \mu\text{m}$ angles. The correspondence here is somewhat better than expected from the errors.

A number of corrections to the total and polarized intensities are needed before the $2.2\ \mu\text{m}$ and radio intensities and polarizations can be quantitatively compared. First is the contamination of the $2.2\ \mu\text{m}$ total intensity by foreground stars in the boxes. The fluxes of the brightest stars in each box were therefore subtracted yielding the "corrected" $2.2\ \mu\text{m}$ intensities given in Table 1. We estimate that the remaining positive star contamination is less than a few percent.

More troublesome are the negative trails from stars in the sky frame, since the contribution from each individual star is spread across the box, and is therefore fainter and harder to recognize. Although the boxes avoid the brightest negative trails, there are certainly unrecognized trails that reduce the $2.2\ \mu\text{m}$ intensities. In individual regions, such as the NW corner of the frame, we can look for negative trails in the absence of bright diffuse emission from Cas A. The distribution of pixel values in that region is consistent with a gaussian distribution around mean zero with a long negative tail. For this region, the negative tail can be recognized and ignored in determining the zero offset level. When negative star trails overlap bright $2.2\ \mu\text{m}$ emission, however, they can reduce the intensity without being recognized. There is thus a negative bias in the $2.2\ \mu\text{m}$ intensities, which we expect to be small on average ($\approx 0.5\mu\text{Jy}/\square''$, or $\approx 5\%$ of the total intensity), but could possibly be as much as $\approx 30\%$ in an individual box, without being recognized. The $2.2\ \mu\text{m}$ total intensity values quoted in Table 1 could therefore actually be somewhat larger, but because of the scientific significance of such larger values, we have taken a more conservative approach and not tried to make any corrections for this possible bias.

Another bias correction that we did *not* make to the data is due to the fact that the sensitive radio observations show that synchrotron emission is present *everywhere* in the $2.2\ \mu\text{m}$ image, and therefore it is not really possible to define an appropriate zero, as discussed earlier. The characteristic intensity of the radio plateau is approximately 15% of the bright ring, so defining it to be zero at $2.2\ \mu\text{m}$ results in spectral indices between $2.2\ \mu\text{m}$ and 6 cm that are too steep by ≈ 0.01 .

Cas A's high optical extinction ($> 4^m$ Searle (1971)) requires that corrections are needed even at $2.2\ \mu\text{m}$. Hurford & Fesen (1996) find reddening of $4.6 < A_V < 5.4$ magnitudes for five FMKs and $A_V = 5.3$ and 6.2 magnitudes for two QSFs, and provide an extensive discussion of the literature on Cas A's extinction. In the west, A_V

² The Very Large Array is an instrument of the National Radio Astronomy Observatory, a National Science Foundation facility operated under cooperative agreement by Associated Universities, Inc.

may extend up to 8 magnitudes, according to the CO and HI analysis of Troland, Crutcher & Heiles (1985). In this paper, we use a value of $A_V = 5$ magnitudes, which leads to $A_{2.2\mu m} = 0.55$ magnitudes, adopting the conversion factors of Bessell, Castelli, & Plez (1998). Application of this extinction value results in the lines labeled “de-reddened” for I, Q, and U in Table 1, and the values plotted in Figure 2. We also show, in Figure 2, the range of corrections that would result for the range $4.6 < A_V < 6.2$ magnitudes.

For any reasonable value of the extinction, it thus appears that the $2.2\mu m$ data consistently fall above the extrapolation from radio wavelengths, giving the spectra a concave shape, i.e., flatter at short wavelengths. There are several caveats to this conclusion. First, a mixture of different power-laws, as observed at cm wavelengths (Anderson & Rudnick 1996; Wright et al. 1999), will result in a concave spectrum. The rms variations within our boxes are ≤ 0.01 , insufficient to cause a significant effect at $2.2\mu m$. However, it is likely that there is some contamination of the bright ring with emission from the steeper spectrum plateau, at least at radio wavelengths. The maximum contamination, for plateau emission with $\alpha_{6cm}^{20cm} = -0.9$ would result in an increase of the $2.2\mu m$ flux density of $\approx 35\%$. The actual $2.2\mu m$ contamination is likely to be considerably lower, given our procedure for setting a zero background, as discussed earlier. However, in any case, this possible contamination is much less than the factor of two enhancement seen at $2.2\mu m$ after correction for extinction.

A second concern is our calibration to the radio flux scale (VLA Calibration Manual 2002), which itself is based on “absolute” calibrations of Cas A (Baars et al. 1977). These two steps are expected to be accurate to $\approx 2\%$, and so could each contribute another 25% error to the $2.2\mu m$ extrapolation. We therefore consider our detection of spectral concavity to be reasonable, but somewhat tentative until the extinction and flux scale issues can be fully resolved. At present, we are analyzing the $6\text{ cm} - 2.2\mu m$ spectra across the whole remnant, which should allow us to use differential measurements to separate real from calibration effects.

3.3. Polarization

The $2.2\mu m$ Stokes parameter values in Table 1 are listed as Q' , U' ; these represent the actual observations, which are only nominally Q and U prior to the calibration of the absolute polarization angle. The properly calibrated polarization position angles are listed in Table 1.

In either the (Q', U') or (Q, U) frame, the observed polarized intensity ($\sqrt{(Q^2 + U^2)}$) represents a biased measure since it would give a positive result from noise, even in the absence of a true signal. As a simple correction for this bias, the fractional polarizations for $2.2\mu m$ listed in Table 1 were calculated as $\%P = [\sqrt{(Q^2 - \sigma_{Q,U}^2 + U^2 - \sigma_{Q,U}^2)}]/I$ where $\sigma_{Q,U}$ were calculated as the rms scatter among boxes of approximately 35 pixels on a side, away from bright stars and away from the bright ring.

For the $2.2\mu m$ polarization measurements, we also need to consider the possible contamination by the foreground interstellar polarization expected from the large extinction towards Cas A. Catalogs of optical polarimetry (e.g. Heiles (2000)) have no stars in the same field as Cas A,

so a direct measurement of the interstellar polarization in the visual has not been made. We have measured the polarization of the bright star in the northwest of our image and find a 3σ upper limit of 0.9% at $2.2\mu m$, although we do not know if it is as far away as Cas A. The expected $2.2\mu m$ polarization for Cas A, given the visual extinction of 5-6 magnitudes, can be estimated using the mean trend in polarization with extinction analyzed in Jones (1989) and Jones, Klebe & Dickey (1991) of

$$\langle P_{2.2\mu m}(\%) \rangle = 2.2 * \tau_{2.2\mu m} = 0.2 * A_V \approx 1\%.$$

Thus, we conclude that interstellar polarization is not a significant contaminant of our polarimetry of the nebulosity at $2.2\mu m$. After consideration of all these effects, and the faintness of the nebulosity being measured, the errors in the fractional polarizations and angles at $2.2\mu m$ are dominated by the random contribution from sky background photons, as opposed to systematic effects. The measured percentage polarizations at $2.2\mu m$ range from $\approx 4 - 10\%$, comparable to those at 6 cm.

To compare the $2.2\mu m$ polarization angles to those at radio wavelengths, we must first correct for Faraday Rotation, which can arise both local to Cas A and along the line of sight. At 20 cm, the rotation is strong enough to actually depolarize the emission (Anderson, Keohane & Rudnick 1995), and render rotation measure (RM) measurements at that wavelength unreliable for the higher frequencies. Kenney & Dent (1985) present RM measurements at low resolution but high frequencies, with a value of -106 rad m^{-2} for the northwestern part of the remnant. In order to look for variations in RM among the boxes used here, we created three different polarization maps at 4.41, 4.64 and 4.99 GHz, using the VLA D configuration data alone to produce a beam size of $\approx 10''$. The signal:noise was insufficient to detect significant variations among the boxes, but averaging over all boxes yields $RM = -105 \pm 3\text{ rad m}^{-2}$, consistent with the Kenney & Dent (1985) value. We therefore adopt the value of -106 rad m^{-2} for all boxes, and show the Faraday corrected position angles in Figure 1 and in the angle comparisons at the bottom of Table 1.

In Figure 3, we compare the position angles of the magnetic fields derived from the polarization vectors in each box with the approximate angles of the filamentary structures in the WFPC2 images of Fesen et al. (2001). All of the position angle measures change systematically with azimuth, with a small but significant clockwise offset from the local radial direction at least for the $2.2\mu m$ and filament angles. It is not clear if the 6 cm angles show any offset, but better local rotation measures would be needed to make the comparison with $2.2\mu m$ angles more accurately.

4. SCIENTIFIC IMPLICATIONS

4.1. Maximum energy of accelerated electrons

Any mechanism to accelerate relativistic particles yields some maximum particle energy. The energy can be limited by a variety of factors including the time available for acceleration, the escape of the highest energy particles from the finite sized acceleration region, or the balance between energy gains and losses (Reynolds 1998, 2001). In Cas A, a hard X-ray tail, which falls two orders of magnitude below the flux extrapolated from radio wavelengths, suggests

that the synchrotron emission may extend to that regime (Allen et al. 1997). This conclusion has been called into question by Bleeker et al. (2001), who argue that the 10 – 15 keV emission is diffuse, and not concentrated at the outer shock as it should be if it were synchrotron. This argument is questionable, however, because the radio synchrotron radiation also does not show an enhancement at the location of the outer shock; X-ray synchrotron emission is therefore still a possibility. Bremsstrahlung provides an alternative explanation for the hard X-ray emission (Laming 2001), where lower hybrid waves in Cas A’s strong magnetic field scatter electrons up to energies of tens of keV. There is not yet any good test to distinguish between bremsstrahlung and synchrotron explanations for Cas A, so the nature of the 10 - 100 keV emission is therefore still open to question. With the demonstration of a synchrotron origin for the 2.2 μm emission, it is therefore interesting to estimate the maximum energy of the accelerated particles.

We start by calculating the value of the field strength that minimizes the energy in both relativistic particles and magnetic field (B_{\min}). We assume a pathlength through the emitting regions of 0.5 pc, with a filling factor of unity. We assume no energy in relativistic protons. These assumptions lead to a field strength of $\approx 500 \mu\text{G}$ for the regions in Table 1. This field strength can then be used to estimate the energy of the relativistic electrons that are radiating at 2.2 μm . In a $\approx 500 \mu\text{G}$ field, this leads to energies of $\approx 150 \text{ GeV}$, or a relativistic gamma of 3×10^5 . As argued below, the synchrotron spectrum almost certainly extends a factor of 10 higher in frequency, which would result in particle energies(gammmas) of $\approx 450 \text{ GeV}$ (9×10^5). This is still a factor of at least 10^3 below energies to which SNRs are commonly expected to accelerate cosmic rays, but it is the first unambiguous demonstration of the extension of the same electron population to such high energies in a shell SNR.

4.2. Synchrotron loss limits

We use the same field strength calculation, and the lack of spectral steepening between 20 cm and 2.2 μm to place a limit on the time since the relativistic particles were last accelerated. The assumptions in the field strength calculation bias the lifetimes to longer values, so our lifetime estimates should be considered upper limits. At a factor of 10 in frequency below the “break” frequency, the spectrum should already have steepened by 0.1 (e.g., Leahy (1991), Figure 3.3a). Since, if anything, the spectra have actually flattened at high frequencies, we adopt 0.1 as a conservative upper limit to the steepening at 2.2 μm , yielding a “break” wavelength of $< 0.22 \mu\text{m}$. This leads to lifetimes for the electrons radiating in the infrared that are no longer than 80 years. It is thus likely that particle acceleration is an ongoing process, at the current stage of Cas A’s evolution. Based on our latest dynamical picture, this is the period when Cas A has probably swept up $\approx 1 - 10$ times its own mass (Gotthelf et al. 2001; Willingale et al. 2002; DeLaney & Rudnick 2002) and during which the reverse shock is slowly coming to the end of its outward motion (in the sky frame). The reverse shock is still strong at this stage, and is encountering outward moving ejecta at speeds of $\approx 5000 - 6000 \text{ km/s}$ (Reed et al. 1995). The

x-ray emitting filaments are rapidly decelerated to $\approx 3500 \text{ km/s}$ while those in the radio are slowed to $\approx 1800 \text{ km/s}$ (Koralesky et al. 1998; Vink et al. 1998; DeLaney & Rudnick 2002); this provides at least one possible source of energy for the relativistic particle acceleration.

4.3. Non-linear shocks

If the acceleration of cosmic rays at SNR shocks is efficient, then there is a back reaction of the cosmic rays on the shock strength and structure (Drury & Völk 1991). When the maximum cosmic ray momentum is limited by shock properties such as geometry, the compression ratio can become arbitrarily large (Eichler 1984). The increasing gyro-radii at higher energies allows those particles to see a higher compression due to the sub-shock structure, so the resulting spectrum becomes concave (Bell 1987; Berezhko & Ellison 1999; Reynolds & Ellison 1992), as observed here. The radio spectra can then be much steeper than the -0.5 expected in the strong shock test particle limit, and can flatten out considerably before they cut off, e.g., in the X-ray, due to radiative losses and escape. Reynolds & Ellison (1992) suggested that slight curvature might have been observed in the integrated radio spectra of Tycho and Kepler SNRs, although the signal was marginal.

In this work, we have shown that the 2.2 μm data, after correction for extinction, fall significantly above the power law extrapolation from the radio. The mean flattening between $\alpha_{20\text{cm}}^{6\text{cm}}$ and $\alpha_{6\text{cm}}^{2.2\mu\text{m}}$ is 0.06 (Table 1), equivalent to higher fluxes at 2.2 μm by a factor of ≈ 2 . If the curvature were constant across this full range of wavelengths, then the **local** spectral index would change from ≈ -0.75 at cm wavelengths to ≈ -0.5 at 2.2 μm . This is essentially the same as the model shown by Berezhko & Ellison (1999). Using their Figure 5, we made a rough calculation of the flux expected at 2.2 μm for Box 1; this is shown as the nested square symbol in Figure 2. The agreement is quite good, suggesting that the signature of acceleration at modified shocks has been observed. In the context of the Berezhko & Ellison (1999) model, this implies a critical injection rate of relativistic particles of $\gtrsim 10^{-4}$ and, for most of the parameters they explored, efficiencies of 10 – 100 %. Thus, with the caveats described earlier regarding the extrapolation of the radio spectrum, relativistic particles appear to be an important part of the dynamics of the shock and the overall evolution of the SNR.

4.4. Polarization

The fractional polarizations and the polarization angles are very similar at 6 cm and 2.2 μm . This provides confirming evidence not only for synchrotron radiation, but that we are looking at the same population of electrons at both wavelengths, validating the detailed spectral comparisons above. The 2.2 μm results confirm the expectation from the Kenney & Dent (1985) mm wave studies that fractional polarizations of $\approx 5 - 10\%$ represent real field disorder, as opposed to Faraday depolarization. Thus, although we speak about the “radial” magnetic fields in Cas A, this only refers to the small net ordered component field. Approximately half of the field energy must be in a component which is disordered on scales $< 1''$ ($< 0.02 \text{ pc}$ at a distance for Cas A of 3.4 kpc).

Gull (1975) first suggested that Rayleigh-Taylor instabilities in the decelerating bright ring of Cas A and other young SNRs would lead to radial magnetic fields. Detailed numerical simulations since that time confirm the prevalence of these filamentary structures and their role in the amplification and alignment of the magnetic fields (Jun & Norman 1996; Jun & Jones 1999). Approximately radial filamentary structures have been seen in the Crab SNR, and, more recently in the WFPC2 images of Cas A (Fesen et al. 2001). In the northwest region investigated here and shown in Fesen et al. (2001) Figure 8, the Cas A filaments emerge from the suggested location of the reverse shock in directions that are systematically non-radial. These non-radial motions could arise from large scale asymmetries in the ejecta, as is well established from the distribution of different elements seen in the X-ray (e.g. Hwang, Holt & Petre (2000)). Alternatively, gradients in the circumstellar medium could cause asymmetric deceleration (e.g. Koralesky et al. (1998)), again leading to large scale velocity shears. In any case, the close correspondence between the R-T finger orientations and the local magnetic field directions strongly supports a connection between the two. Blondin & Ellison (2001) show that the R-T instabilities generated at the reverse shock can extend all the way out to the outer shock front, providing radial magnetic fields instead of the tangential ones otherwise expected at the shock. The transition region between the radial and tangential regions may have been observed in Cas A (Gotthelf et al. 2001), although the signal-to-noise is quite low.

5. CONCLUSIONS

The extension of Cassiopeia A's known synchrotron spectrum to 2.2 μm opens up a variety of important issues

regarding the acceleration of relativistic particles. First, we have established that the acceleration mechanism, usually assumed to be diffusive acceleration at shocks, operates to energies of at least 150 GeV in Cas A. In addition, there is reasonable evidence that these shocks are efficient particle accelerators, arising from non-linear interactions between the particles and the shocks. This creates the opportunity to investigate these interactions in conjunction with the dynamical information about the several coupled plasmas (thermal and non-thermal) in the remnant. In turn, this will strongly constrain models for the high X-ray energy tail in Cas A's spectrum and assist in the challenge of isolating the energy in relativistic protons. To make progress on these issues, a detailed investigation of the radio/2.2 μm spectral shape as a function of the radio spectral index variations across the remnant is underway. The association of magnetic fields with the local R-T instabilities opens the door for investigating the accompanying amplification of magnetic fields in the remnant, and the roles of both relativistic particles and fields in the further dynamical evolution of the remnant.

We appreciate the 2.2 μm images provided by C. Gerardy and R. Fesen, and a number of important discussions on the science with Tom Jones. Support for work on Cas A at the University of Minnesota was provided by National Science Foundation grant AST-96-19438 and for comparisons with HST data by NASA through grant number HST-AR-090537.01-A from the Space Telescope Science Institute, which is operated by the Association of Universities for Research in Astronomy, Inc., under NASA contract NAS5-26555. The comments of the referee were very helpful in improving the paper.

REFERENCES

Allen, G. E., Keohane, J. W., Gotthelf, E. V., et al. 1997, *ApJ*, 487, L97
 Anderson, M. C. & Rudnick, L. 1996, *ApJ*, 456, 234
 Anderson, M. C., Keohane, J. & Rudnick, L. 1995, *ApJ*, 441, 300
 Baars, J. W. M., Genzel, R., Pauliny-Toth, I. I. K., & Witzel, A. 1977, *A&A*, 61, 99
 Bell, A. R. 1978, *MNRAS*, 182, 147
 Bell, A. R. 1987, *MNRAS*, 225, 615
 Berezhko, E. G. & Ellison, D. C. 1999, *ApJ*, 526, 385
 Bessell, M. S., Castelli, F. & Plex, B. 1998, *A&A*, 333, 231
 Bleeker, J. A. M., Willingale, R., van der Heyden, K., Dennerl, K., Kaasstra, J. S., Aschenbach, B., & Vink, J. 2001, *A&A*, 365, L225
 Blandford, R. D., & Eichler, D. 1987, *Phys. Rep.*, 154, 1
 Blondin, J. M. & Ellison, D. C. 2001, *ApJ*, 560, 244
 Borkowski, K. J., Rho, J., Reynolds, S. P., & Dyer, K. K. 2001, *ApJ*, 550, 334
 DeLaney, T. & Rudnick, L. 2002, in preparation.
 Drury, L. & Völk, H. 1981, *ApJ*, 248, 344
 Eichler, D. 1984, *ApJ*, 277, 429
 Elias, J. H., Frogel, J. A., Matthews, K., & Neugebauer, G. 1982, *AJ*, 87, 1029
 Fesen, R., Morse, J., Chevalier, Roger A.; Borkowski, Kazimierz J.; Gerardy, Christopher L.; Lawrence, Stephen S.; van den Bergh, S. 2001, *AJ*, 102, 122
 Gerardy, C. & Fesen, R. 2001, *AJ*, 121, 2781
 Gotthelf, E. V., Koralesky, B., Rudnick, L., Jones, T. W., Hwang, U. & Petre, R. 2001, *ApJ*, L552
 Green, D. 2001, "A Catalog of Supernova Remnants," <http://www.mrao.cam.ac.uk/surveys/snrs>
 Gull, S. F. 1975, *MNRAS*, 171, 263
 Heiles, C. 2000, *AJ*, 119, 923
 Hurford, A. P. & Fesen, R. A. 1996, *ApJ*, 469, 246
 Hwang, U., Holt, S. S. & Petre, R. 2000, *ApJ*, 537, L119
 Jones, T. J. 1989, *ApJ*, 346, 728
 Jones, T. J. 1997, *AJ*, 114, 1393
 Jones, T. J. 2000, *AJ*, 120, 2920
 Jones, T. J., Klebe, D., & Dickey, J. 1991, *ApJ*, 386, 602
 Jun, B-I, Norman, M. L. 1996, *ApJ*, 472, 245
 Jun, B-I, Jones, T. W. 1999, *ApJ*, 511, 774
 Kassim, N. E. 1989, *ApJ*, 347, 915
 Kassim, N.E., Perley, R. A., Dwarakanath, K.S. & Erickson, W. C., 1995, *ApJ*, 455, L59
 Kenney, J. D. & Dent, W. A. 1985, *ApJ*, 298, 644
 Kobayashi, Y., Kawara, K., Maihara, T., Okuda, H., Sato, S. & Noguchi, K., 1978, *PASJ*, 30, 377
 Koralesky, B., Rudnick, L., Gotthelf, E. V. & Keohane, J. W. 1998, *ApJ*, 505, 27
 Koyama, K., Petre, R., Gotthelf, E. V., et al. 1995, *Nature*, 378, 255
 Koyama, K., Kinugasa, K., Matsuzaki, K., et al. 1997, *PASJ*, 49, L7
 Lagage, P. O., Claret, A., Ballet, F., Boulanger, Cesarsky, C. J., Cesarsky, D., Fransson, C., and Pollock, A. 1996, *A&A*, 315, L273
 Laming, J. M. 2001, *ApJ*, 546, 1149
 Leahy, D. & Roger, R. S. 1998, *ApJ*, 505, 784
 Leahy, J. P. 1991, in "Beams and Jets in Astrophysics," ed. P. A. Hughes, (Cambridge Univ. Press: Cambridge), 100
 Muraishi, H., Tanimori, T., Yanagita, S. et al. 2000, *A&A*, 354, L57
 NRAO VLA Calibration Manual, <http://www.aoc.nrao.edu/vla/html/vlahome/astronomer.html>
 gtaylor/Calib
 Reed, J. E., Hester, J. J., Fabian, A. C., & Winkler, P. F. 1995, *ApJ*, 440, 706
 Reynolds, S. P. 1996, *ApJ*, 459, L13
 Reynolds, S. P. 1998, *ApJ*, 493, 375
 Reynolds, S. P. 2001, *SSRv*, 99, 177
 Reynolds, S. P. & Ellison, D. C. 1992, *ApJ*, 399L, 75
 Reynolds, S. P. & Keohane, J. 1999, *ApJ*, 525, 368
 Rudnick, L. 2002, *PASP*, 114, 427
 Rudnick, L. & Jones, T. W. 1983, *AJ*, 88, 518
 Searle, L. 1971, *ApJ*, 168, 41
 Slane, P., Gaensler, B. M., Dame, T. M., Hughes, J. P., Plucinsky, P. & Green, A. 1999, *ApJ*, 525, 357
 Tanimori, T., Hayami, Y., Kamei, S. et al. 1998, *ApJ*, 497, L25
 Troland, T. H., Crutcher, R. M & Heiles, C. 1985, *ApJ*, 298 808

Tuffs, R. J., Drury, L., Fischera, J., Heinrichsen, I., Rasmussen, I., Russel, S. & Völk, H. 1997, Proc. of first ISO workshop on Analytical Spectroscopy, ESA SP 419, p 177

Vink, J., Bloemen, H., Kaastra, J.S. & Bleeker, J. A. M 1998, A&A, 339 201

Weintraub, D. A. & Kastner, J. 1993, ApJ, 411, 767

Willingale, R., Bleeker, J A. M., van der Heyden, K. J., & Kaastra, J. S. 2002, astro-ph/0207273

Wright, M., Dickel, J., Koralesky, B. & Rudnick, L. 1999, ApJ, 518, 284

TABLE 1
INTENSITY AND POLARIZATION MEASUREMENTS

	Box 1	Box 2	Box 3	Box 4	Box 5	Box 6	Units (Error)
Azimuth	-10	-20	-30	-35	-42	-32	degrees
$I_{2\mu m}$ observed	12.0	18.6	7.6		13.5	12.8	$\mu\text{Jy}/\square''$ (0.26)
$I_{2\mu m}$ corrected	11.0	9.6	7.6		9.3	12.8	$\mu\text{Jy}/\square''$ (0.26)
$I_{2\mu m}$ de-reddened	18.3	15.9	12.6		15.4	21.2	$\mu\text{Jy}/\square''$ (0.43)
$Q'_{2\mu m}$ observed	-0.67	-0.48	-0.54	-0.84	-0.84	-0.48	$\mu\text{Jy}/\square''$ (0.2)
$Q'_{2\mu m}$ de-reddened	-1.11	-0.80	-0.90	-1.4	-1.4	-0.8	$\mu\text{Jy}/\square''$ (0.3)
$U'_{2\mu m}$ observed	-0.34	.041	0.33	0.42	0.50	1.0	$\mu\text{Jy}/\square''$ (0.2)
$U'_{2\mu m}$ de-reddened	-0.56	.068	0.55	0.70	0.83	1.66	$\mu\text{Jy}/\square''$ (0.3)
% $P_{2\mu m}$	6.2	3.8	7.2		9.9	8.3	(1.5)
$PA_{2\mu}$	70	55	41	44	42	57	degrees (13)
I_{20cm}	56,800	53,800	63,900	56,300	63,300	61,600	$\mu\text{Jy}/\square''$ (300)
I_{6cm}	21,500	20,400	24,200	21,500	23,500	23,200	$\mu\text{Jy}/\square''$ (100)
Q_{6cm}	-144	51	258	780	1535	163	$\mu\text{Jy}/\square''$ (45)
U_{6cm}	1400	965	1550	1270	700	680	$\mu\text{Jy}/\square''$ (45)
% P_{6cm}	6.5	4.7	6.5	6.9	7.2	3.0	(0.2)
PA_{6cm}	48	43.5	40.3	29.2	12.2	38.2	degrees (2)
$\approx PA$ (filaments)	-40	-40	-33	-70	-78	-33	degrees (15)
COMPARISONS							
% $P_{2.2\mu m}/\%P_{6cm}$	0.95	0.81	1.11		1.38	2.8	(0.2)
$PA_{6cm}(corr) - PA_{2\mu}$	-10	-1.5	+11	-3	-18	-7	degrees (13)
α_{20cm}^{6cm}	-0.76	-0.75	-0.76	-0.75	-0.77	-0.76	(.01)
$\alpha_{2.2\mu m}^{6cm}$	-0.69	-0.70	-0.73		-0.71	-0.68	(< .01)

Note: The absolute position angle (PA) on the sky at $2.2\mu m$ is $(0.5 \times \tan^{-1} \frac{U'}{Q'} - 33)$ degrees. In the top section, the 6 cm PAs are as observed, *not* corrected for Faraday rotation. For comparison with the $2.2\mu m$ PAs in the bottom section, a correction for a rotation of -106 rad m^{-2} has been applied.

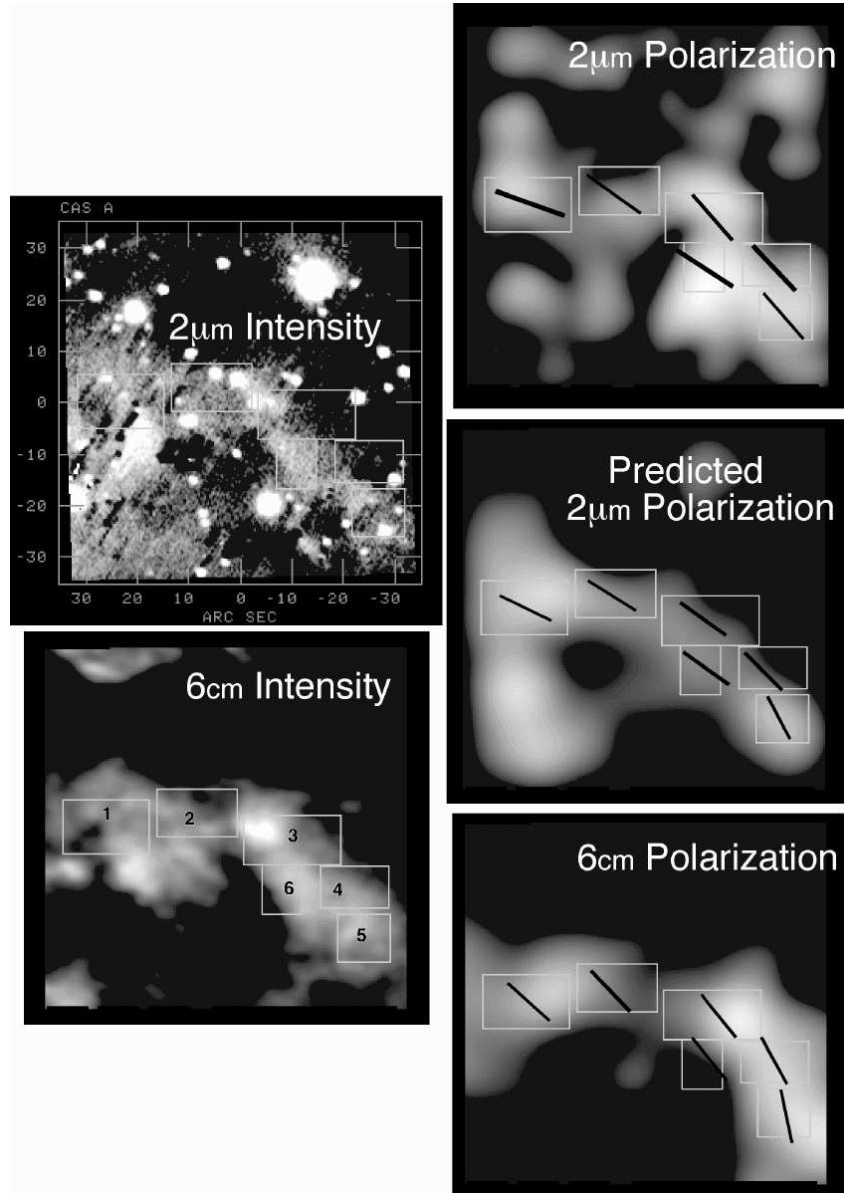


FIG. 1.— Total intensity and polarization for Cassiopeia A at $2.2 \mu\text{m}$ and 6 cm . The left side images of total intensity are at resolutions of $1''$ (approximate seeing) and $1.5''$, respectively. The center of all images is at RA $23\text{h} 23\text{m} 26\text{s}$, Dec $58^\circ 48' 58.4''$, (J2000), and the scale is shown on the $2.2 \mu\text{m}$ map. The images on the right are of polarized flux, convolved to $10''$, along with the angle of the *electric field* (observed PA) for the boxes listed in Table 1. The middle frame on the right shows the predicted $2.2 \mu\text{m}$ polarization predicted from the radio measurements, as described in the text.

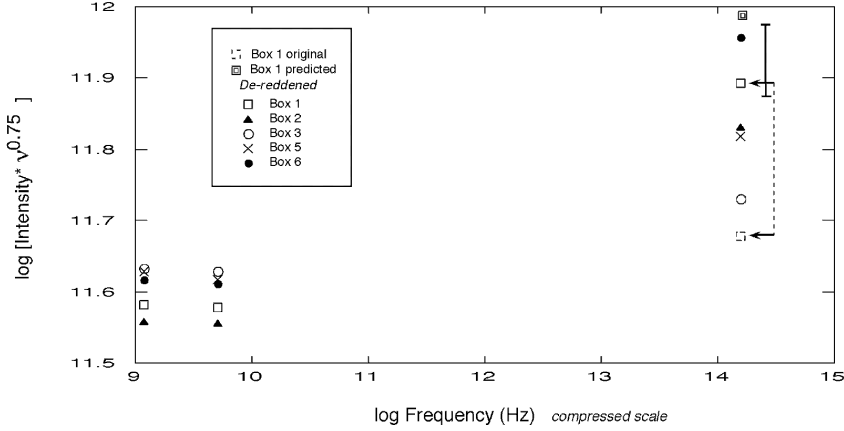


FIG. 2.— Flux densities for five of the boxes shown in Table 1, as a function of frequency. The flux densities have been multiplied by a factor of $\nu^{0.75}$ to accentuate the curvature. The errors in the radio are smaller than the symbol sizes. The errors at $2.2\mu\text{m}$ are dominated by uncertainties in the extinction correction. The open and closed squares and the dashed line connecting them show the size of the nominal extinction correction applied to each box. The error bar on the right shows the range of possible extinction corrections that could have been applied to the square (Box 1), as per the text discussion. The embedded squares show a prediction for Box 1 based on non-linear acceleration at modified shocks, again as described in the text.

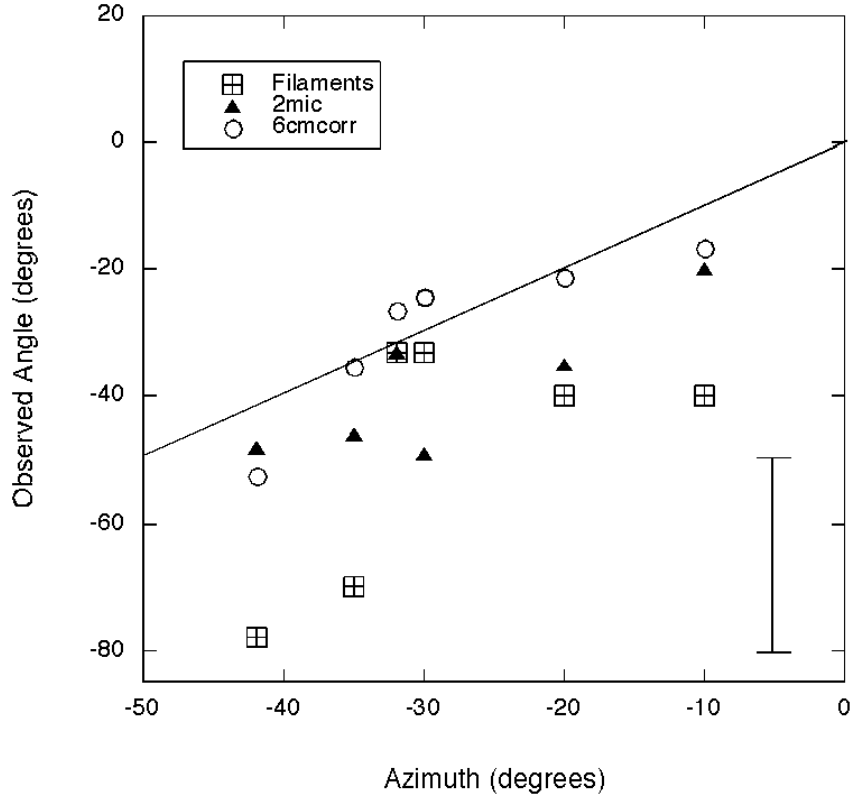


FIG. 3.— Inferred magnetic field angles (observed PA + 90 deg) and filament position angles as a function of azimuth. A characteristic error is shown for the 2.2 μ m polarization and optical filament angles. The 6 cm angles have been corrected for the average RM in this region of -106 rad/m² and have errors of approximately the symbol size. The line indicates pure radial alignment.